Fines Mobility and Distribution in Streaming Fibre Networks: Experimental Evidence and Numerical Modeling

Supplementary Material

Experimental Set-Up and Visual Characterization of the Fibre Suspension Flow

Parameter Fitting and Validation of the Numerical Model

Jakob D. Redlinger-Pohn[*1,3], Melanie Mayr[2], Gregor Schaub[1], David Gruber[1], and Stefan Radl[1]

[1]Institute of Process and Particle Engineer, Graz University of Technology, Austria
[2]Institute of Bioproducts and Paper Technology, Graz University of Technology, Austria
[3]Department of Engineering Mechanics, KTH Royal Institute of Technology, Sweden

[*]Author e-mail address: edu.redlinger@gmail.com

1. FIBRE PULP AND VISUAL CHARACTERIZATION OF FIBRE SEGREGATION OF STREAMING NETWORKS

1.1. Fibre Pulp

Three types of pulps (SW, L100, S100), and two mixtures (L90S10, L50S50) were used in this study. Their volume-based fibre-length distribution ΔQ_3 (Fig. S1) was calculated from fibre-length measurement with a L&W Fibretester+ (ABB, Lorentzen & Wettre, Sweden) assuming cylindrical shape. The fibre classes were defined as [0.0, 0.2, 0.6, 1.0, 2.0, 3.0, 4.0, 5.5] mm.

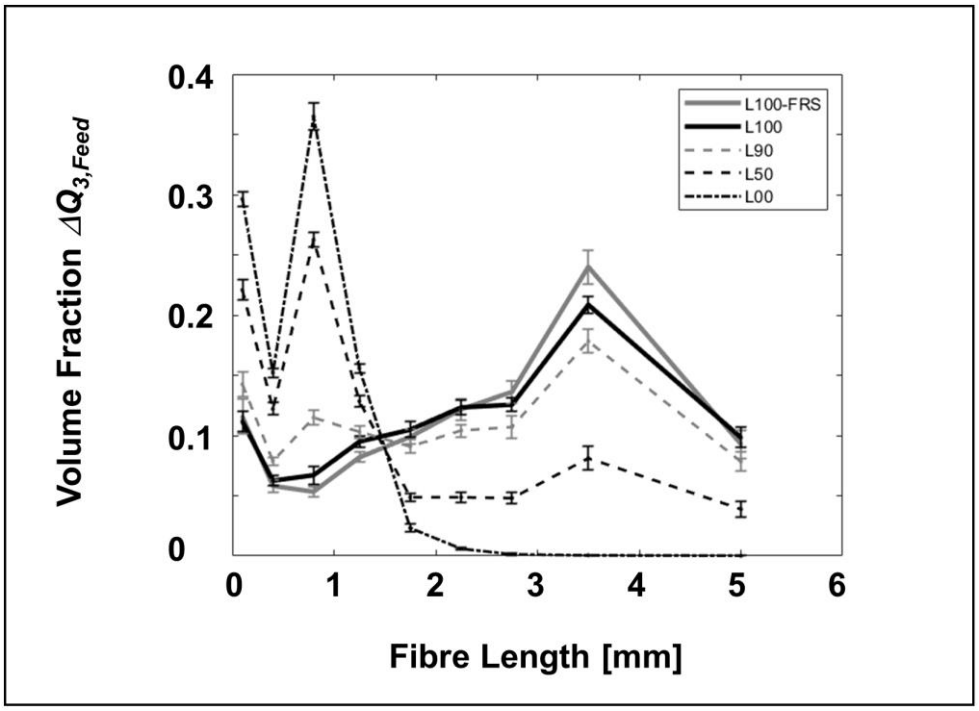

Fig. S1 Volume-based (ΔQ_3) length distribution of the fibre pulp used in this study. SW (grey solid) and L100 (black solid) are softwood pulps from two different sources (Sappi Gratkorn and Zellstoff Pöls, respectively). S100 (black dash-dotted) is a hardwood pulp (Sappi Gratkorn). L90S10 (grey dashed) and L50S50 (black dashed) are mixtures of L100 and S100 with 90% and 50% softwood, respectively.

The first class, from 0.0 to 0.2 mm with the class mean of 0.1 mm represents the fibre-fines in the sample. SW (soft wood pulp) is unrefined chemical sulphite pulp, 100% spruce, bleached and washed, provided by Sappi Gratkorn (Austria). L100 (soft wood pulp) is a fully bleached unrefined mixture of 90% spruce, and 10% pine provided by Zellstoff Pöls (Austria). S100 (hard wood pulp) is a non-further specified mixture of European and American eucalyptus provided by Sappi Gratkorn (Austria). L90S10, and L50S50 are mixtures of L100 and S100 with 90% and 50% L100, respectively. S100 (eucalyptus pulp) is a pulp of shorter fibres which

was mixed into L100 (spruce) to reduce the network strength and increase the number of fibres in the range of 1 mm.

1.2. Visual Characterized Fibre Segregation of Streaming Networks

The imaging results and imaging processing performed for experiments with SW, soft-wood pulp were reported previously in Redlinger-Pohn et al. (Redlinger-Pohn et al. 2017):

Images were recorded with a high-speed camera (IDT Os8-S3, Imaging Solution GmbH, Germany) at a resolution of 1600x1200 pixel (width x height), covering an area of 0.71H times 0.53H. H is the normalized channel height. The imaging frequency was adjusted to the flow rate, to take approximately two pictures per time needed for the pulp to pass through the observed length. This procedure guarantees a fair comparison of different cases, i.e., an identical amount of fibres was captured for all experiments. A snapshot for each case is shown in **Fig. S2**a-d. The images were averaged resulting to a greyscale image with high intensitites for high fibre concentration (**Fig. S2**e-h). The network-gap and network-annulus interface was taken from a sharp change in the slope value of the grey intensity curve (**Fig. S2**) under consideration of what can be seen in the raw images (**Fig. S2**a-d). The fibre network was captured for one half of the channel, ca. 0.47H from the wall into the suspension.

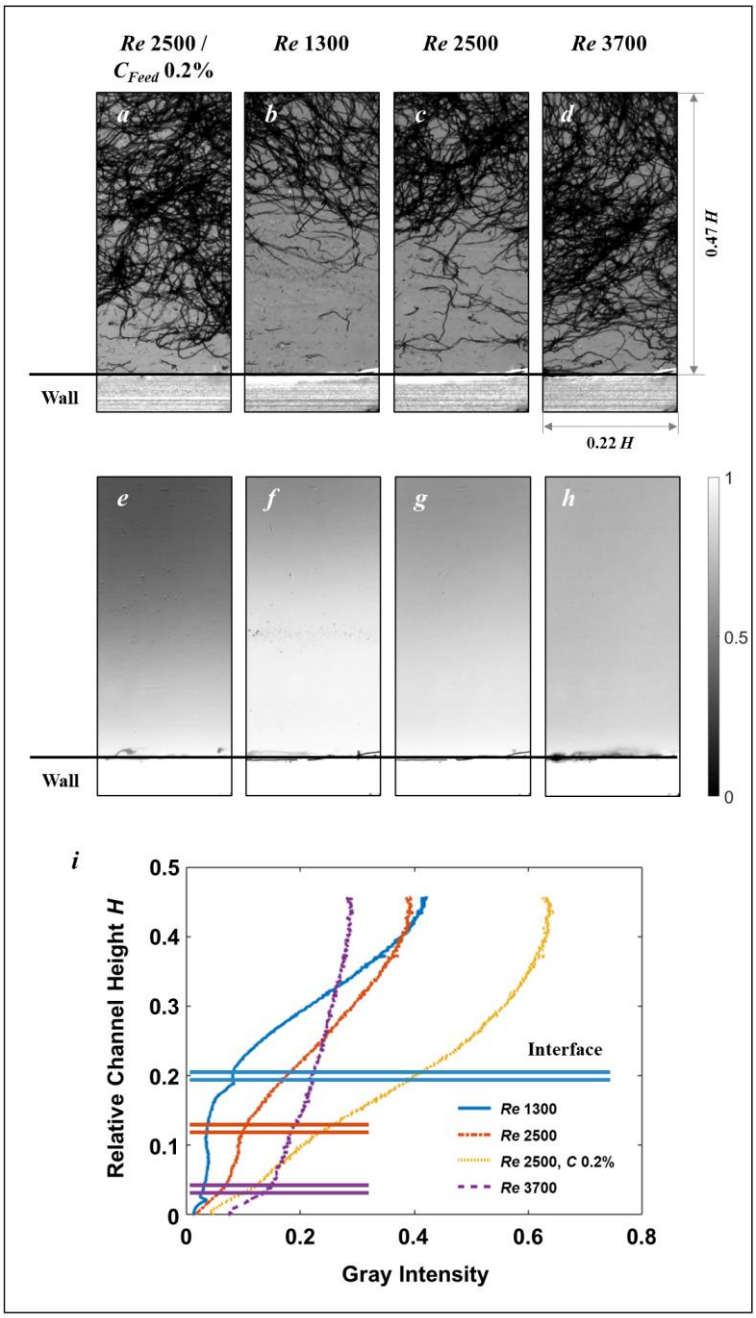

Fig. S2 Fibre distribution in the channel along *H* (Redlinger-Pohn et al. 2017). Shown is the lower half (0.47*H*) of a symmetric channel. a-d are snapshots showing the fibre aggregation and, in cases, segregation in the channel centre. e-h are the corresponding gray images from 3600 averaged images. i shows the gray intensity in wall-normal direction. The double line indicated the network interface identified from the change in gray intensity slope.

2. FIBRE MIGRATION MODEL DEVELOPMENT AND VALIDATION

2.1. Case Description

We follow the process and pipe parameters presented in Cotas et al. (Cotas et al. 2017). Specifically, a cylindrical pipe with a length of L=1 m, and a radius of R=0.05 m was considered. The flow was considered axisymmetric, hence the flow in the wedge-shaped geometry illustrated in **Fig. S3** was studied (for mesh parameters the caption of this figure). At the inlet a block profile and a uniform concentration distribution was considered. In case a turbulence model was used, a turbulent intensity of 5% (for the turbulent kinetic energy) and a turbulent mixing length of 0.02 m was considered (these parameters were adopted as typical engineering guess, and did not influence simulation results). All simulations were initialized with a laminar velocity profile at the desired inlet flow speed (see left panel of **Fig. S3**).

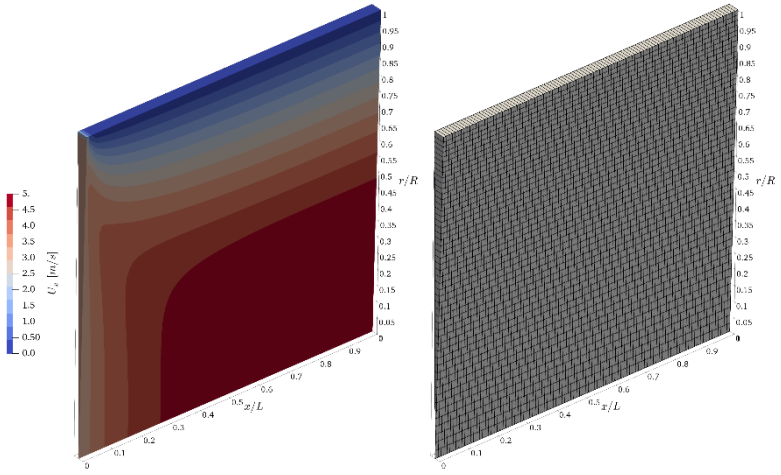

Fig. S3 Illustration of the computational domain used for model development (the left panel illustrates a typical initial velocity profile used for the simulations. The right panel illustrates the computational grid with 100x50 cells in the axial and radial direction was used, respectively. The grid was compressed in the radial direction by a factor of 0.6).

For the viscosity model we adopt the parameters summarized in **Table S1** that have been extracted from Cotas et al. for pine pulp.

Table S1 Fitting functions for the coefficients in the Herschel-Bulkley viscosity model used by Cotas et al. (pine pulp; note that the original prefactor for τ_0 is 7.94, but this prefactor considered the fibre concentration to be in percent)

Parameter	
τ_0 **[Pa]**	$y = 1.148 \cdot 10^5 \cdot c^{2.08}$
k **[Pa]**	$y = 0.0754 \cdot (c \cdot 100)^{5.90} + 10^{-3}$
n **[-]**	$y = \max(0.01, 1 - 28.0 \cdot c)$

2.1.1. Screening of Influencing Factors

Dynamic versus Dynamic-Elastic Fibre Drift Flux Modeling

The closure for the fibre migration speed $\mathbf{u}_{drift}$ has in total six influence parameters in case one lumps the fibre projected area A_f with the drift coefficient K_{drift} (i.e., we introduce the dynamic drift strength parameter $K = A_f K_{drift}$). We next highlight the effect of key parameters of the fibre drift flux model in the absence of a turbulence model (i.e., assuming a laminar flow).

Initial simulations showed that for the two exponents $n_{c,drag}, n_c$ the value of zero should be adopted (specifically, the motivation of choosing $n_{c,drag}$ is motivated by the resulting singularity at $c = 0$). Moreover, for the shear rate exponent n_{SR} the value of unity was chosen. Performing simulations with different values for the dynamic drift strength K shows that this parameter controls the thickness of the layer void of fibres near the channel wall. Consequently, a value of $K = 10^{-7}$ m² was adopted for all simulations that follow.

The results of the screening of the remaining two parameters (i.e., $K_{el}, n_{c,E}$) are summarized in Fig. S4. As can be seen, not including an elastic stress component (i.e., setting $K_{el} = 0$) leads to a local concentration of fibres at a distance $r/R \sim 0.1$ from the wall (see the right panel of **Fig. S4**). Such an fibre accumulation is not observed experimentally by Cotas et al. (Cotas et al. 2017) (see the EIT measurements in their Fig. 10). Also, choosing n_{CE} as unity or two has no effect on the velocity and fibre concentration profiles, as long as the elastic drift strength parameter K_{el} is adjusted accordingly. Considering the left panel of **Fig. S4**, one can observe that the present model predictions do not agree - even qualitatively - with that of Cotas et al. (Cotas et al. 2017). Next, we questioned the assumption of laminar flow (and not using a turbulence model).

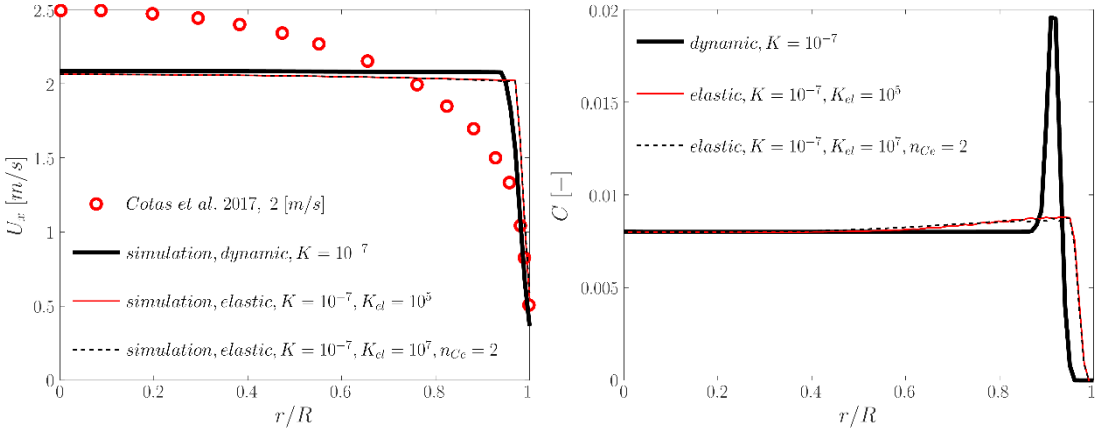

Fig. S4 Radial profiles of the axial suspension velocity (left panel), as well as of the fibre concentration (right panel) for different settings of the fibre migration model (if not otherwise stated, K_{el} = 0 1/s, and $n_{c,E}$ = 0; fibres from pine wood).

Turbulence Model

After choosing the most realistic model parameters for the fibre migration model, all available low-Reynolds turbulence models in the used CFD software (i.e., OpenFOAM® 5.x) were analyzed. Results for four representative turbulence models are summarized in **Fig. S5**.

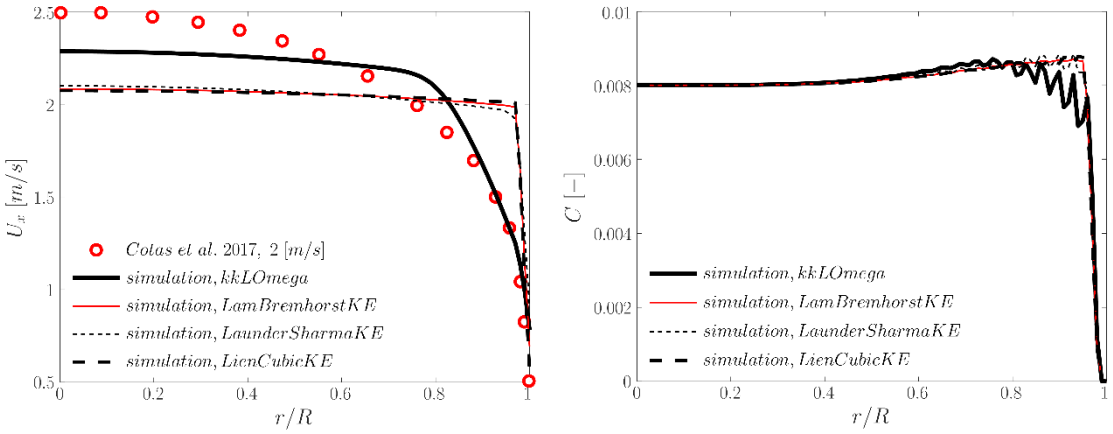

Fig. S5 Radial profiles of the axial suspension velocity (left panel), as well as of the fibre concentration (right panel) for different low-Reynolds turbulence model (K_{el} 2; fibres from pine wood).

As can be seen, only the kkLOmega turbulence models has a substantial effect on the velocity and concentration profile. Only this model leads to a velocity profile close to that of Cotas et al. (Cotas et al. 2017). The fibre concentration profile shown in **Fig. S5** (right panel) suggests that this improvement is to an erosion of the central fibre plug that moves through the cylindrical pipe. This is supported by the profile for the turbulent viscosity displayed in **Fig.**

S6, which indicates a substantial turbulent stress in the order of 10^{-4} m²/s in the flow for the kkLOmega turbulence model.

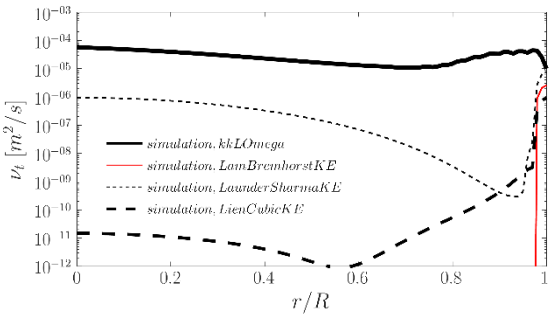

Fig. S6 Radial profiles of the turbulence viscosity for four representative low-Reynolds turbulence models (K_{el} = 10^7 1/s, and $n_{c,E}$ = 2; fibres from pine wood, U_{in} = 2 m/s).

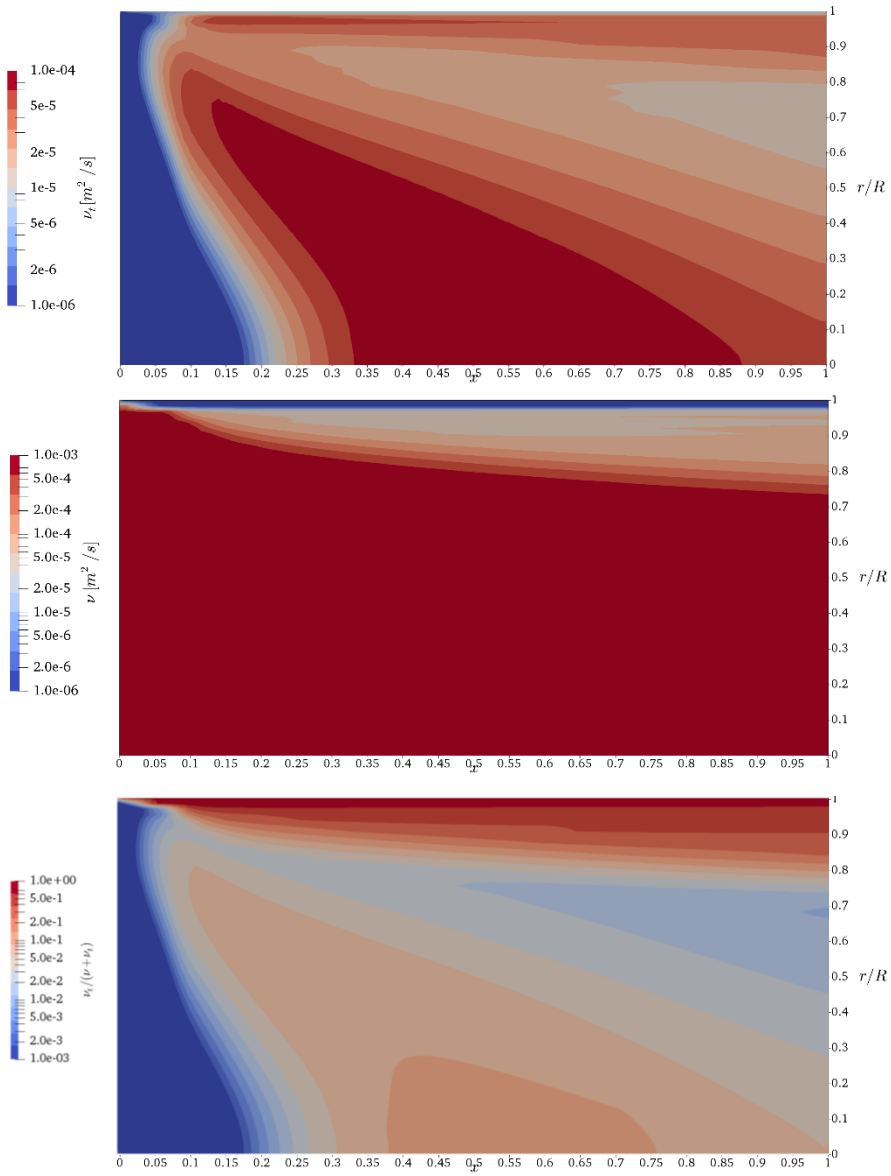

Fig. S7 Contour plot of the suspension's viscosity (top panel), turbulence viscosity (center panel), as well as the contribution of the turbulence viscosity to the total viscosity (bottom panel) for U_{in} = 2 m/s (the flow is from left to right; K_{el} = 10^7 1/s, and $n_{c,E}$ = 2; fibres from pine wood; kkLOmega turbulence model).

The comparison of suspension's kinematic and turbulence viscosity in **Fig. S7** (bottom panel) indicates that in the wall-near region these viscosities (and hence the resulting stresses) are comparable. Directly at the wall the turbulent stresses even exceed that due to the suspension viscosity, and hence dominate.

2.1.2. Benchmarking at Higher Suspension Speed and Fibre Concentration

Simulations at an inlet speed of U_{in}=3 m/s, as well as an almost double fibre concentration (i.e., C = 1.5%; note that Cotas et al., did not report velocity profiles for this concentration, hence we report only our predictions) yield reasonable agreement with the data provided by Cotas et al. (Cotas et al. 2017).

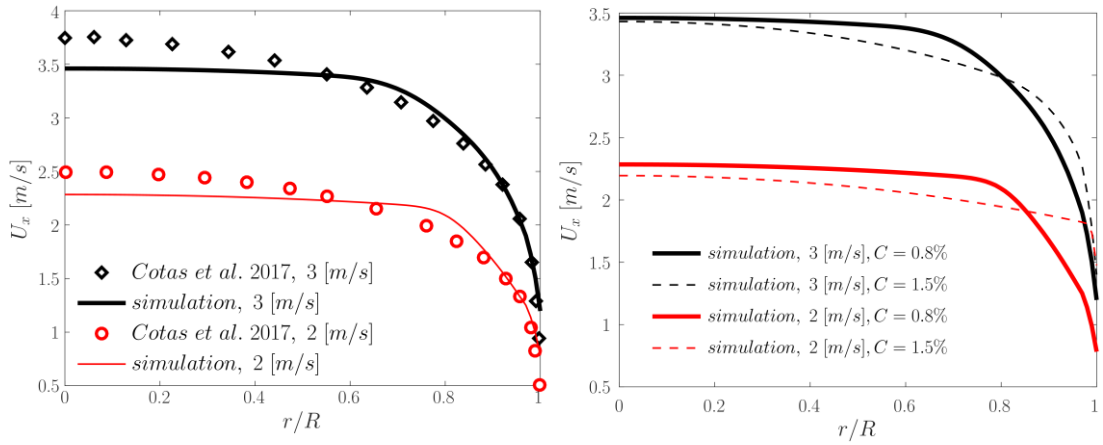

Fig. S8 Velocity profiles for various inflow velocities and fibre concentrations (K_{el} = 10^7 [1/s], and $n_{c,E}$ = 2; fibres from pine wood; the left panel documents data for C = 0.8%; the right panel illustrates velocity and concentration effects).

2.2. Grid Convergency Study

2.2.1. *Cotas* et al. *Cases*

We analysed the effect of the grid resolution for selected cases (i.e., a consistency of 0.8% and flow speeds of 2 and 3 [m/s]) presented by Cotas et al. for grid parameters summarized in **Table S2**.

Table S2 Grid resolutions used to investigate grid convergency (Cotas et al. cases; $n_{cells,ax}$ and $n_{cells,r}$ is the number of grid points in the axial and radial direction, respectively. All grids were compressed in the radial direction by a factor of 0.6 towards the wall)

$n_{cells,ax}$	$n_{cells,r}$	*remark*
25	50	
50	100	Base case
75	150	
113	225	
170	338	

Results for 2 [ms]

As can be seen in **Fig. S9**, the largest effect of grid resolution near the wall. This is the region in which the turbulence viscosity is most significant. There exists an appreciable effect of the grid resolution on the velocity profile, which is especially important between r/R = 0.85 …1 (see top right panel in **Fig. S9**). Extremely fine grids (i.e., $n_{cells,r}$ 225 and 338) capture the formation of an extremely thin wall-near layer at approximately r/R = 0.99. In this wall-near layer the velocity gradient is extremely large, which is only captured by the two finest grids.

For concentration profiles grid effects are only significant for r/R = 0.95 …1. For the finest and coarsest grid it is observed that the concentration profile near the wall is steadily increasing with increasing wall distance. All other grids indicate a thin layer (i.e., for r/R > 0.99) that is free of fibres.

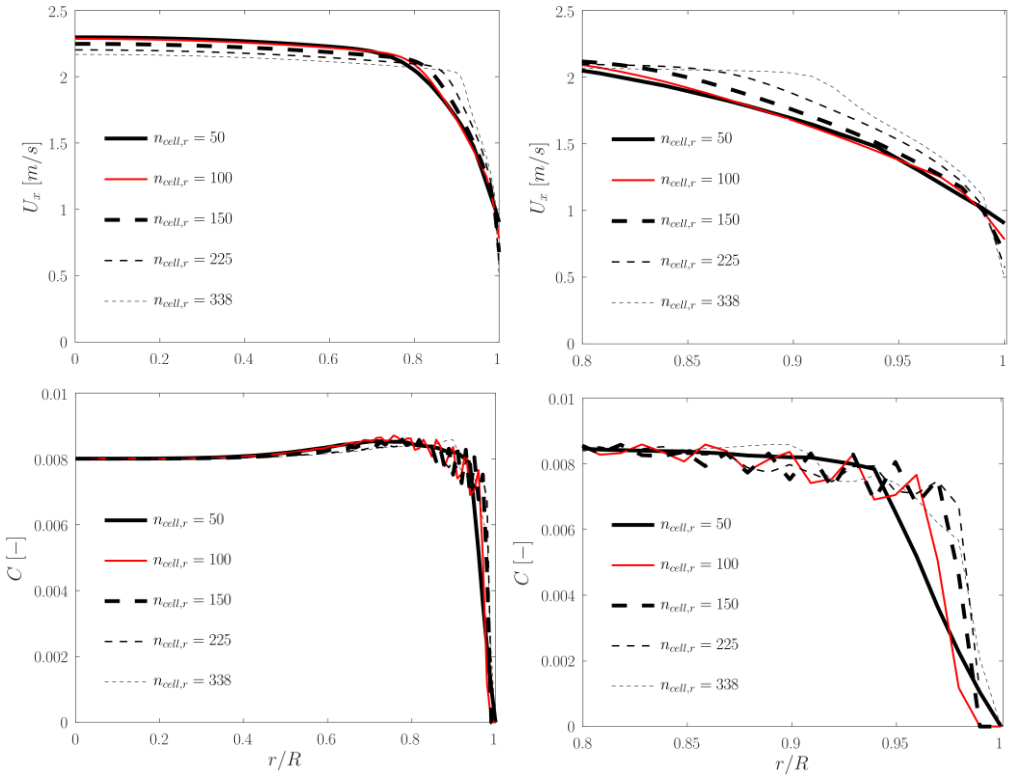

Fig. S9 Velocity (top panels) and concentration profiles (bottom panels) summarizing the results of the grid sensitivity analyis (U_{in} = 2 m/s, C = 0.8%; the right panel are close-ups fo the wall-near region).

Results for 3 [ms]

Similar grid effects as for the lower speed of 2 [m/s] were observed. However, as can be seen in Fig. S10, these effects are less pronounced for the case of 3 [m/s]. All grids except the coarsest one indicate the formation of a thin layer (i.e., for $r/R > 0.99$) that is free of fibres.

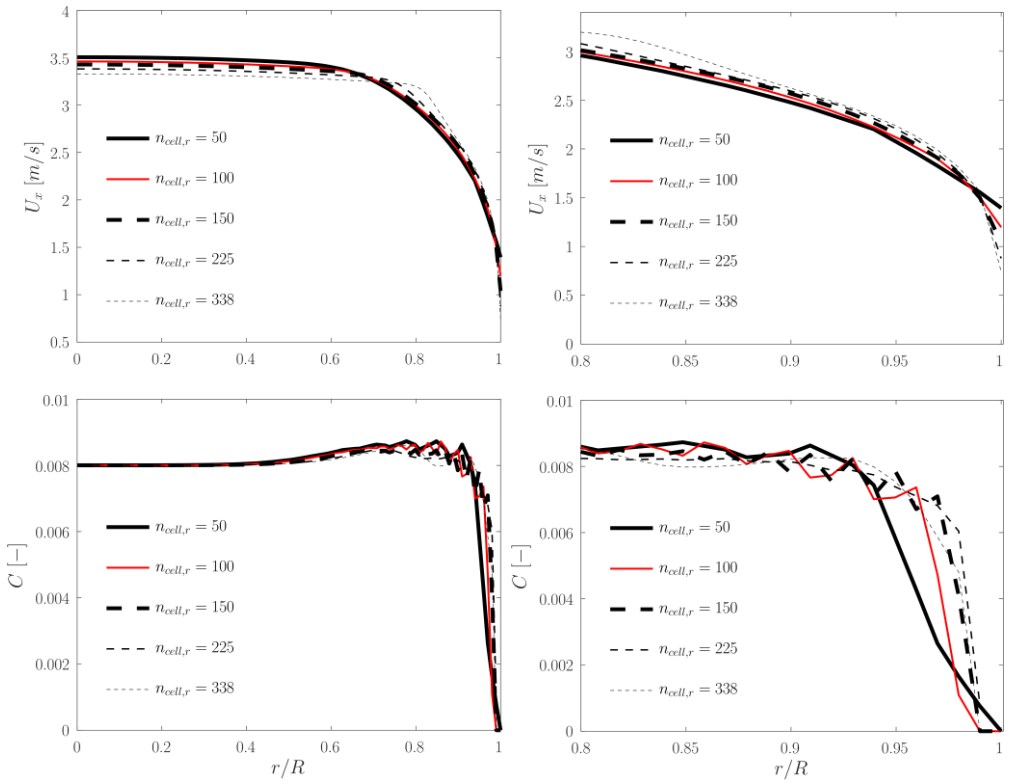

Fig. S10 Velocity (top panels) and concentration profiles (bottom panels) summarizing the results of the grid sensitivity analyis (U_{in} = 3 m/s, C = 0.8%; the right panel are close-ups fo the wall-near region).

2.2.2. 3D Cases

We analysed the effect of the grid resolution for as a selected case (i.e., C = 0.1% and Re = 3700) and for grid parameters summarized in **Table S3**. Note in passing that the resolutions in y- and z-direction are for the the half width and height, respectively.

No qualitative differences in the velocity and concentration profiles (see **Fig. S11**) could be detected. Our data for the velocity profile shows minimal deviations, only in the wall-near region the slope of velocity profile is not exactly matched: finer grids indicate higher velocity gradients that are resolved near the wall.

Our data for the concentration profile shows that fine grids lead to a more pronounced maximum of the concentration located at y/H = 0.25. The thickness of the fibre-free layer near the wall is relatively insensitive to the grid resolution, and reasonably predicted by all our simulations.

Table S3 Grid resolutions used to investigate grid convergency (3D case; $n_{cells,x}$, $n_{cells,y}$ and $n_{cells,z}$ is the number of grid points in the axial, y- and z-direction, respectively. All grids were compressed in the y- and z-direction by a factor of 0.6 towards the wall)

$n_{cells,x}$	$n_{cells,y}$	$n_{cells,z}$	*remark*
140	18	7	
200	25	10	Base case
300	38	15	
450	57	23	

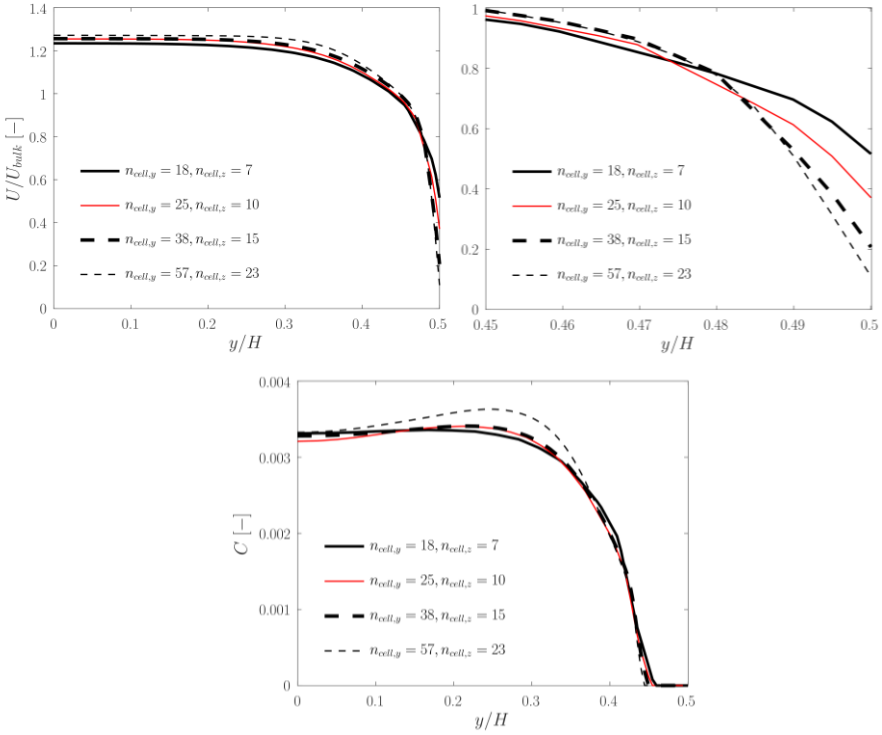

Fig. S11 Velocity (top panels; the right panel is a close-up near the wall) and concentration profiles (bottom panel) summarizing the results of the grid sensitivity analyis (3D case, C = 0.1%, Re = 3700; data is shown for z = 0, i.e., the center plane of the channel).

2.2.3. 2D Cases

We analysed the effect of the grid resolution for selected cases (i.e., C = 0.1% and 0.2%, as well as Re = 1300 and 7400) and for the grid parameters summarized in **Table S4**. We note in passing that the resolutions in the y-direction is for the the half width of the channel only.

Table S4 Grid resolutions used to investigate grid convergency (2D cases; $n_{cells,x}$ and $n_{cells,y}$ is the number of grid points in the axial, and span direction, respectively. All grids were compressed in the span direction by a factor of 0.6 towards the wall).

$n_{cells,x}$	$n_{cells,y}$	*remark*
133	17	
200	25	Base case
300	38	
450	57	
450	86	Only for case C = 0.2%, Re = 7400

Results for low Reynolds number flow (*Re *= 1300) and C = 0.1%

Our data indicates a clear grid convergence of simulation results for the lowest Reynolds number and concentration (see **Fig. S12**). While our simulation with the coarsest grid already predicts the velocity and concentration profile reasonably well (see the bold solid line in **Fig. S12**), the velocity field in the wall-near region is not accurately predicted. Also, the coarsest grid cannot predict the extremely high concentration gradient at approximately y/H = 0.35 that is observed in the grid-converged solution. However, as can be seen in **Fig. S12**, all features of velocity and concentration profile are predicted reasonably well with all computational meshes used.

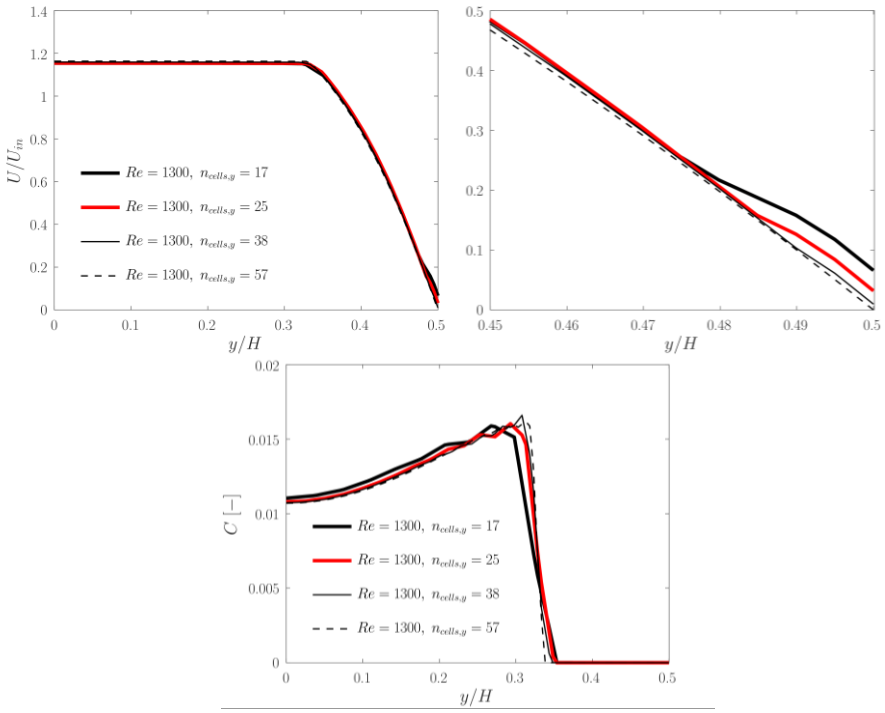

Fig. S12 Velocity (top panels; the right panel is a close-up near the wall) and concentration profiles (bottom panel) summarizing the results of the grid sensitivity analyis (2D case, C = 0.1%, Re = 1300).

*Results for high Reynolds number flow (***Re** *= 7400) and C = 0.1%*

Velocity profiles (see top panels in Fig. S13) show a consistent behaviour over wide range of span-wise positions. However, near the wall, the steep velocity gradients are better resolved by the high resolution simulations. This is in line with our observations made for the lower Reynolds number.

Concentration profiles (see bottom panels in **Fig. S13**) show a consistent behaviour as well, except for the highest resolution: for this case a qualitative change in the concentration oscillations in the region $y/H < 0.35$ is observed. However, the extend of the fibre-free region near the wall is predicted consistently for all simulations featuring different resolutions.

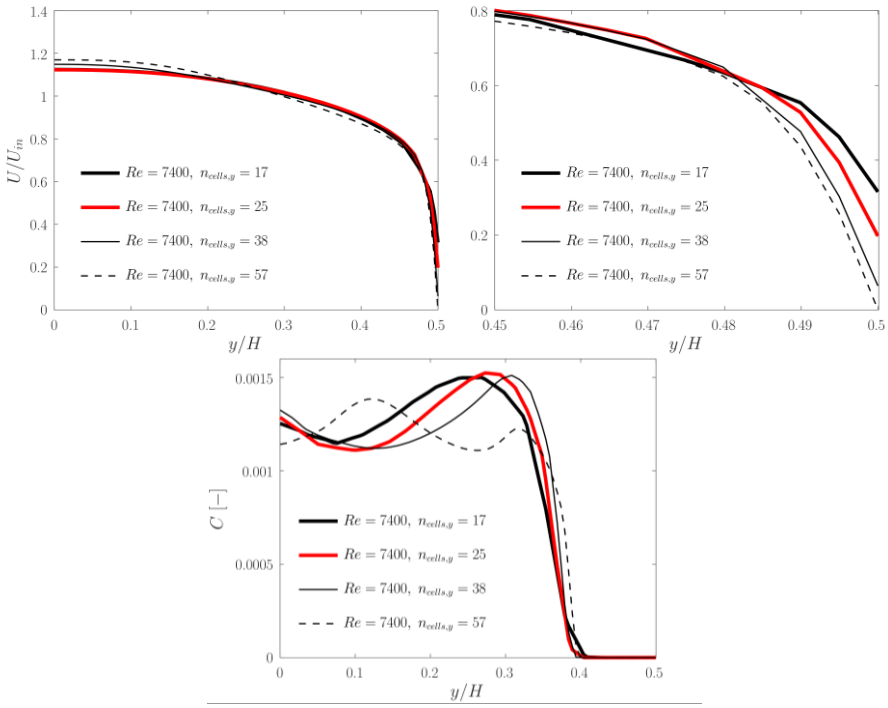

Fig. S13 Velocity (top panels; the right panel is a close-up near the wall) and concentration profiles (bottom panel) summarizing the results of the grid sensitivity analyis (2D case, C = 0.1%, Re = 7400).

*Results for high Reynolds number flow (***Re** *= 7400) and C = 0.2%*

Similar observations as for the data at C=0.1% can be made (see **Fig. S14**): again, trends for the velocity profiles follow a consistent trend with increasing grid resolution, with higher predictions for the velocity gradient near the wall in case of a finer computational mesh.

However, the simulation at extremely high resolution (i.e., $n_{cell,y}$ = 86) indicates unrealistic oscillations in the concentration field. This suggest that for the highest grid resolutions (i.e., $n_{cell,y}$ = 57 … 86) one should be carefuly with interpreting oscillations in the concentration field. We were unable at the moment to evaluate if these oscillations are physical, or originate from the assumptions in our mathematical model.

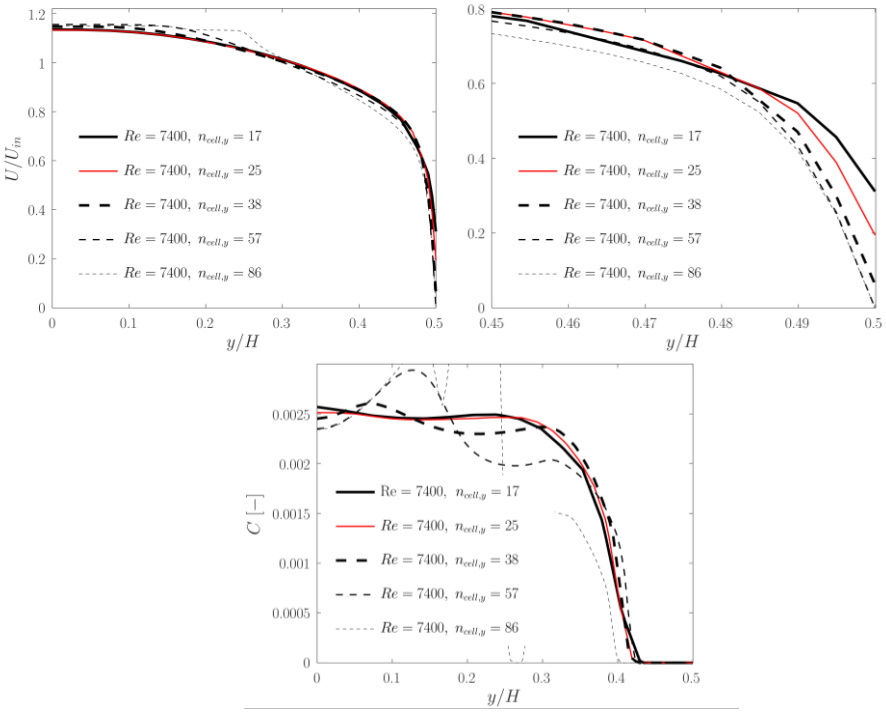

Fig. S14 Velocity (top and center panels) and concentration profiles (bottom panels) summarizing the results of the grid sensitivity analyis (2D case, C = 0.2%, Re = 7400).

3. REFERENCE FOR CITATIONS IN THE SUPPLEMENT MATERIAL

Cotas C, Branco B, Asendrych D, et al (2017) Experimental Study and Computational Fluid Dynamics Modeling of Pulp Suspensions Flow in a Pipe. J Fluids Eng 139:. https://doi.org/10.1115/1.4036165

Redlinger-Pohn JD, Bauer W, Radl S (2017) Fractionation of fibre pulp in a hydrodynamic fractionation device: influence of reynolds number and accept flow rate. Trans 16Th Fundam Res Symp Held Oxford Sept 2017 209–228